Solid-State Structural Evolution of Poly(ethylene terephthalate) During Step Uniaxial Stretching from Different Initial Morphologies: An *In Situ* Wide Angle X-ray Scattering Study

Lyudmil V. Todorov, Carla I. Martins, Júlio C. Viana

Department of Polymer Engineering, Institute for Polymers and Composites/I3N, University of Minho, 4800-058 Guimarães, Portugal

Received 13 February 2011; accepted 13 April 2011
DOI 10.1002/app.34706
Published online 5 October 2011 in Wiley Online Library (wileyonlinelibrary.com).

ABSTRACT: This work reports an *in situ* wide-angle X-ray scattering (WAXS) study of the structural evolution of PET with distinct initial morphologies during step uniaxial stretching in the solid state. Two types of samples were analyzed under synchrotron X-ray radiation, namely quasi-amorphous (QA) and semicrystalline (SC) (with 2D and 3D order). Results show that initially different QA morphologies evolve following the same stages: (i) stage I (before neck), at almost constant orientation level the amorphous phase evolves into mesophase; (ii) stage II (neck formation), there is a rapid increase of polymer orientation and the appearance of a periodical mesophase from the highly oriented mesophase; (iii) stage III (necking propagation), there is a leveling off of the average polymer orientation together with partial conversion of the periodical mesophase and mesophase into highly oriented amorphous. The behaviors of the two SC morphologies are completely distinct. A 2D order crystalline morphology evolves with stretching likewise the QA through three stages: (i) at early stages of deformation the polymer orientation remains unchanged while the amorphous phase amount increases slightly, stage I; (ii) in stage II, a fast increase of polymer orientation is accompanied by large formation of mesophase; and (iii) in stage III there is the level off of polymer orientation as the chains approach their finite extensibility and the 3D crystalline order is achieved. Evolution of SC sample with 3D crystalline order mainly features constant orientation increase together with mesophase increment. Structure deformation models are suggested. © 2011 Wiley Periodicals, Inc. J Appl Polym Sci 124: 470–483, 2012

Key words: crystal structures; drawing; morphology; WAXS

INTRODUCTION

Poly(ethylene terephthalate) (PET) is the unquestioned leader among thermoplastic polyesters regarding its industrial applications.[1] PET is slowly crystallizing thermoplastic polyester that can be obtained with different morphologies, either an amorphous or a semicrystalline (SC) when cooled from the melt, depending on the cooling rate applied. Once rapidly quenched into its amorphous state, PET structure can be developed by: (i) stretching in the rubbery state (above T_g), which leads to high polymer orientation and strain-induced triclinic crystalline structure development[2,3] and/or by (ii) stretching in the solid state (at room temperature) resulting in extraordinarily large chain orientation without actual crystallization, but developing a strain-induced mesomorphic phase, the mesophase.[4,5] Both pathways lead to strain-induced structural development that improves mechanical and physical properties, determined by the imposed thermomechanical environment during stretching.[6–8] The structural evolution mechanisms taking place during the stretching requires *in situ* characterization techniques as synchrotron X-ray diffraction. The structure evolution is of academic and industrial interest and from extreme importance under processing and in-service conditions.

Ex situ[2,6,7,9–23] and *in situ*[24–34] synchrotron X-ray scattering have been used to characterize the PET structural evolution during the uniaxial stretching in the rubbery state. Gorlier et al.[21] proposed a three-stage structure development mechanism (SDM). More recently, the SDM was correlated to the superstructure by *in situ* Small Angle X-ray Diffraction (SAXS)/wide-angle X-ray scattering (WAXS),[35,36] by

Correspondence to: J. C. Viana (jcv@dep.uminho.pt).

Contract grant sponsor: DESY, European Commission; contract grant numbers: HASYLAB Project DESY-D-II-05-101 EC, the FP6 contracts RII3-CT-2004-506008 (IA-SFS), project APT_PACK-SRTP-505204-1.

Contract grant sponsor: Portuguese Foundation for Science and Technology, FCT; contract grant number: Microtest-POCTI/CTM/46940/2002.

Contract grant sponsor: Ph.D. Student grant; contract grant number: SFRH/BD/44917/2008.

TABLE I
Structure Parameters Calculated from the 2D WAXS Patterns

	Parameter								
							Crystallite size		
Samples	f_{av}	f_{am}	f_c	Amor [%]	Meso [%]	Cryst [%]	(100) [Å]	(010) [Å]	(−103) [Å]
QA1	0.05	0.28	–	64.7	35.3	0.0	–	–	–
QA2	0.07	0.30	–	88.3	11.7	0.0	–	–	–
SC1	0.18	0.55	0.58	28.4	34.6	37.0	24	38	–
SC2	0.47	0.67	0.65	36.5	23.2	40.3	20	36	26

f_{av}: average polymer orientation; f_{am}: amorphous phase orientation; f_c: crystallite orientation; Amor: amorphous phase; Meso: mesophase; Cryst: crystalline mass fraction; (100), (010), and (−103) crystalline plains).

the following stages: (i) first stage, called "orientation," involves the formation of mesophase from oriented chain segments and formation of microfibrillar structure; (ii) second, "nucleation" stage, involves the initiation of crystallization from the mesophase through nucleation and growth processes, forming imperfect crystals with 2D order; and (iii) third, "growth" stage, corresponds to the stable crystal growth phase with 3D order. The lamellar superstructure is responsible for the linear load increase, enabling a good lattice PET triclinic unit cell to be registered. PETs triclinic unit cell is described with $a = 4.62$ Å, $b = 5.92$ Å, $c = 10.68$ Å, $\alpha = 99.8°$, $\beta = 127.6°$, and $\gamma = 104.9°$.[37]

During stretching in the solid state, amorphous PET develops in a mesophase without crystallization to occur. Mesophase was first reported by the pioneer studies of Bonart.[4,5] Auriemma et al.[38] associated the meridional peak, (00−1) corresponding to $d = 10.3$ Å, to the mesophase, which has a smaller monomer length than the typical PET unit cell ($c = 10.7$ Å). Asano et al.[39] reported that stretching of amorphous PET in the solid state results in the formation of an oriented nematic phase, with alternating position of the phenylene rings on neighboring molecules. After annealing at 60°C nematic transforms into smectic phase (00−1) $2\theta = 8.56°$ ($d = 10.7$ Å) with neighboring rings aligned on the plane perpendicular to the stretching direction and slightly tilted on the molecule axis. Other works reported the meridional peak (10−3) appearance at $2\Theta = 25.8°$.[7,40] Ran et al.[41] interpreted the emergence of this peak to the mesophase formation with similar packing symmetry to the crystalline phase with 3D crystalline order[35,42] that is described by meridional crystalline unit cell reflection (−103) at $2\Theta = 26.6°$.[40]

The present study aims at contributing for a deeper understanding on the PET structure evolution upon uniaxial step stretching in the solid state by *in situ* WAXS characterization from distinct initial morphologies. For that purpose two types of morphologies were studied: (i) two quasi-amorphous (QA) samples with different orientation level and phase's fractions and (ii) two SC samples with 2D crystalline order and the other with 3D order. The mechanism of structure evolution and effect of initial morphologies are discussed.

EXPERIMENTAL

Material

Poly(ethylene terephthalate) with intrinsic viscosity of 0.74 ± 0.02 dL g^{-1}—bottle grade, solid density of 1.40 g cm^{-3} and approximate average molar mass, M_n, of 20,000 g mol^{-1} was used in this study.

Samples

The samples used in this work were prepared following the procedure described in a previous work.[43] In summary, PET pellets were compression molded and quenched to obtain amorphous plaques. The plaques were cut with a dumbbell-like shape and uniaxially deformed in the rubbery state following a stretching program, where stretching rate ($\varepsilon_{st} = 0.003$ and 0.03 s^{-1}), stretching temperature ($T_{st} = 90$ and 110°C), and stretching ratio ($\lambda_{st} = 1.6\times$ and $2.1\times$) were varied. Different morphologies were obtained through this procedure: two QA and two SC samples. These samples were then cut into rectangular tensile bars with the dimensions of: length of rectangular part of 25 mm and cross section of 4 mm × 0.3 mm, to perform the solid-state deformation simultaneous to the *in situ* X-ray characterization.

Structural parameters of the initial samples, as revealed by WAXS analyses, are listed in Table I. For clear identification of the samples, the following nomenclature has been adopted:

(i) quasi-amorphous samples, QA1 and QA2. The main differences between them are the orientation level and content of phase's mass fractions, in which QA1 has a greater amount of mesophase and slightly lower orientation level than the QA2.

(ii) semicrystalline samples, SC1 and SC2. The SC2 sample is more oriented than SC1, and shows a crystalline phase with 3D order, indicated by the meridional crystalline peak reflection (−103), while in case of SC1 this peak is absent, showing a 2D crystalline order.

Solid-state stretching and *in situ* WAXS characterization

Solid-state stretching was carried (at controlled room temperature of 23°C) simultaneously to *in situ* WAXS experiments under synchrotron radiation at HASYLAB, DESY, Hamburg (A2 soft condensed matter beam-line) with incident X-ray beam, monochromatized by reflection from a bent Ge (111) single crystal ($\lambda = 0.15$ nm). A Microtester, micro-universal testing apparatus, developed by our group[44] was used to perform the uniaxial stretching. The PET samples were clamped between jaws of the Microtester (distance between tie bar 25 mm) with its center positioned perpendicularly to the X-ray beam, at a sample-to-detector distance of 135 mm and the stretching direction pointing upward. The Microtester was employed in tensile mode with simultaneous movement of the grips apart from each other to the maximum stretching ratio of 1.5×, the limit of apparatus. The stretching protocol was as follows:

(i) clamp the sample in the stretching machine and start the deformation process (typical stretching rate of 10^{-3} s^{-1});
(ii) after some deformation the stretching was ceased and allowed a 2-min pause at constant strain,
(iii) in meanwhile acquire the 2D WAXS pattern with an accumulation time of 20 s,
(iv) restore the stretching procedure.

This step-wise procedure results in some molecular relaxation that affects the morphology development. The comparison between the continuous and step-wise protocols was reported elsewhere.[45] The use of step wise result in higher level of amorphous phase orientation, in case of both morphologies, is related to a better rearrangement of the mesophase during the relaxation over the interrupted deformation period. On the other hand, stretching stopping contributes for better defined 2D WAXS patterns.

The WAXS was calibrated with the different diffractions of a crystalline PET sample. Background scattering was subtracted and all plots were normalized with respect to the incident X-ray intensity, accumulation time, and specimen thickness. Actual specimen's thickness was obtained by first approximation of a homogeneous deformation, in which sample thickness changes with the stretching ratio, λ, according to the following equation[46]:

$$t = t_0 \lambda^{-1/2} \quad (1)$$

where t—actual sample thickness and t_0—initial sample thickness.

WAXS data analysis

Phase mass fraction

The two linear intensity profiles, taken along the equatorial and meridional directions from the 2D WAXD patterns were used to estimate mass fractions of the phases. A peak-fitting program using a Gaussian function was used to deconvolute the phase's peaks. Studied samples have two different particular morphologies: (a) QA and (b) SC. Therefore, two specific data analyses procedures were adopted for the calculations of the phase's mass fractions. These methodologies are described below.

Quasi-amorphous morphologies. The morphology of QA samples was assumed to consist of two main phases: (i) amorphous—isotropic phase and (ii) mesophase—anisotropic phase with degree of packing and order between the crystalline and the amorphous. The amount of amorphous phase was assumed to be proportional to the area of the linear meridional profile. The subtraction of the amorphous fractions from the total area in the equatorial profile was proportional to the amount of the mesophase. The mass fractions of the individual phase were taken as the ratio of the area for each phase to the total area of the equatorial profile. As the strain increases, the WAXS patterns can exhibit a pair of meridional mesomorphic reflection (10−3) at about $2\Theta = 25.8°$,[7,40] indicating conformational regularity, and called periodical mesophase (PM). At this stage of deformation, the QA samples morphologies were considered to be composed of three phases: (i) amorphous (ii) mesophase, and (iii) periodical mesophase—mesophase with conformational periodicity perpendicular to the stretching direction. The area of fitted (10−3) peak profile was used to determine the mass fraction of the PM. The sum of the area convoluted under the equatorial intensity profile and the meridional (10−3) peak was assumed to be the total area. The mass fractions of the individual phase were taken as the ratio of the area for each phase to the total area.

Semicrystalline morphologies. The morphology of initially SC samples was assumed to contain three distinct phases[31]: (i) amorphous—isotropic phase, (ii) mesophase—which has a degree of packing order between the crystalline and the amorphous phase,

and (iii) a crystalline (triclinic) phase. The amount of crystalline phase was assumed to be proportional to the total area of the deconvoluted peaks (010): at $2\theta = 17.3^\circ$, (−110) at $2\theta = 22.5^\circ$, and (100) at $2\theta = 25.7^\circ$ from the linear equatorial profile, whereas, the amount of the unoriented amorphous phase was assumed to be proportional to the area of the linear meridional profile. When a crystal diffraction peak was detected in the meridional profile, i.e., (−103) at around $2\theta = 26^\circ$, its area contribution was excluded.[31] The subtraction of the crystalline and amorphous fractions from the total area of the equatorial profile was considered to be proportional to the amount of the mesophase. The mass fraction of the individual phases was taken as the ratio of the area for each phase to the total area of the equatorial profile.

Polymer molecular orientation

Average polymer molecular orientation. The WAXS patterns were integrated along an azimuthal angle of $\mu = 0 - \pi/2$ ($\mu = 0$ at equator), over a section with a $2\Theta = 13$–28°, to calculate the average polymer molecular orientation, f_{av}. That sector encloses all possible crystal reflections of crystallographic planes, isotropic amorphous phase, and mesophases of PET.[14] The Hermans' orientation function was used to evaluate the f_{av}[47]:

$$f = \frac{3\langle \cos^2 \phi \rangle - 1}{2} \tag{2}$$

where the $\langle \cos^2\phi \rangle$ is defined as:

$$\langle \cos^2 \phi \rangle = \frac{\int_0^{\pi/2} I(\phi) \cos^2 \phi \sin \phi d\phi}{\int_0^{\pi/2} I(\phi) \sin \phi d\phi} \tag{3}$$

where ϕ is the azimuthal angle, I is the diffracted intensity and $\langle \cos^2\phi \rangle$ is the average angle that the normal makes with the principal deformation direction.

Amorphous phase molecular orientation. Amorphous phase molecular orientation, f_{am}, was determined from the azimuthal scans obtained over $\mu = 2\pi$ ($\mu = 0$ at equator) between 2Θ values of 19.3° and 20.8°.[18] This annular ring is located between the (010) at $2\theta = 17.3^\circ$ and (−111) at $2\theta = 21.2^\circ$ crystalline reflections, that is an angular range where the amorphous peak is reasonably intense and has least overlap from the crystalline reflections, when such are present. The profiles were fitted to Gaussian peaks and a horizontal baseline. The width of the peak was used to calculate the f_{am} using [eqs. (2) and (3)]. The $<\cos^2\phi>$ was evaluated by the full-width at half maximum ($\Delta\phi$) of the Gaussian peak intensity distribution, by $\langle \cos^2\phi \rangle$ integrated between $\pi/2$ and $-\pi/2$ for each value of $\Delta\phi$ from the relation:

$$I(\phi) = \exp\left(\frac{-4\phi^2 \ln 2}{\Delta\phi^2}\right) \tag{4}$$

Crystalline phase orientation. Crystalline phase orientation, f_c, of PET in terms of the angle σ between the *c*-axis of the unit cell and the stretching direction can be characterized by the normal to the (−105) lattice plane as well as by using the three equatorial reflections, (010), (−110), and (100) according to the Wilchinsky's method.[48] The (−1,0,5) reflection is found to occur at a large scattering angle, $2\Theta = 43^\circ$,[14] which is out of the characterized sector. Using Wilchinsky's method[14,48] to determine the crystallite orientation of PET, the $\langle \cos^2\sigma \rangle$ can be calculated from the experimental $\langle \cos^2 \phi_{hk0} \rangle$ [eq. (3)] of the three equatorial reflections, by the following equation:

$$\langle \cos^2\sigma \rangle = 1 - A\langle \cos^2\phi_{010} \rangle - B\langle \cos^2\phi_{-110} \rangle - C\langle \cos^2\phi_{100} \rangle \tag{5}$$

where the parameters $A = 0.8786$, $B = 0.7733$, and $C = 0.3481$ are derived from the triclinic crystal system.[32] The $\langle \cos \phi_{hkl} \rangle$ values were obtained by eq. (3) for each peak reflection and substituted in eq. (5), to obtain $\langle \cos^2\sigma \rangle$, which was used to calculate the f_c by means of eq. (2).

Crystallite dimensions

The apparent crystal sizes normal to the three crystalline reflections, (100), (010), and (−103), which are almost orthogonal to each other, were estimated by the analysis of the linear intensity profiles taken across the reflection peaks. The vector normal (100) is coincided with that of benzene stacking, the vector normal (010) is approximately parallel to the benzene ring and the appearance of the (−103) peak indicates ordering along the stretching axis. Thus crystalline dimensions[31,49,50] was estimated using the Scherrer equation:

$$D_{hkl} = K\lambda / \left(\beta_{1/2} \cos\Theta\right) \tag{6}$$

where D_{hkl} represents the apparent lateral crystallite size of the *hkl* reflection plane, $\beta_{1/2}$ is the full width at the half height of the diffraction peak *hkl* in radians, the shape factor K is set at 0.9 for polymer systems, λ is the X-ray wavelength ($\lambda = 1.54$ Å), and Θ is half of the diffraction angle. There is the possibility of lattice distortion, which would broaden the line width, leading to the underestimation of the crystal size. According to Kawakami et al.,[49] based

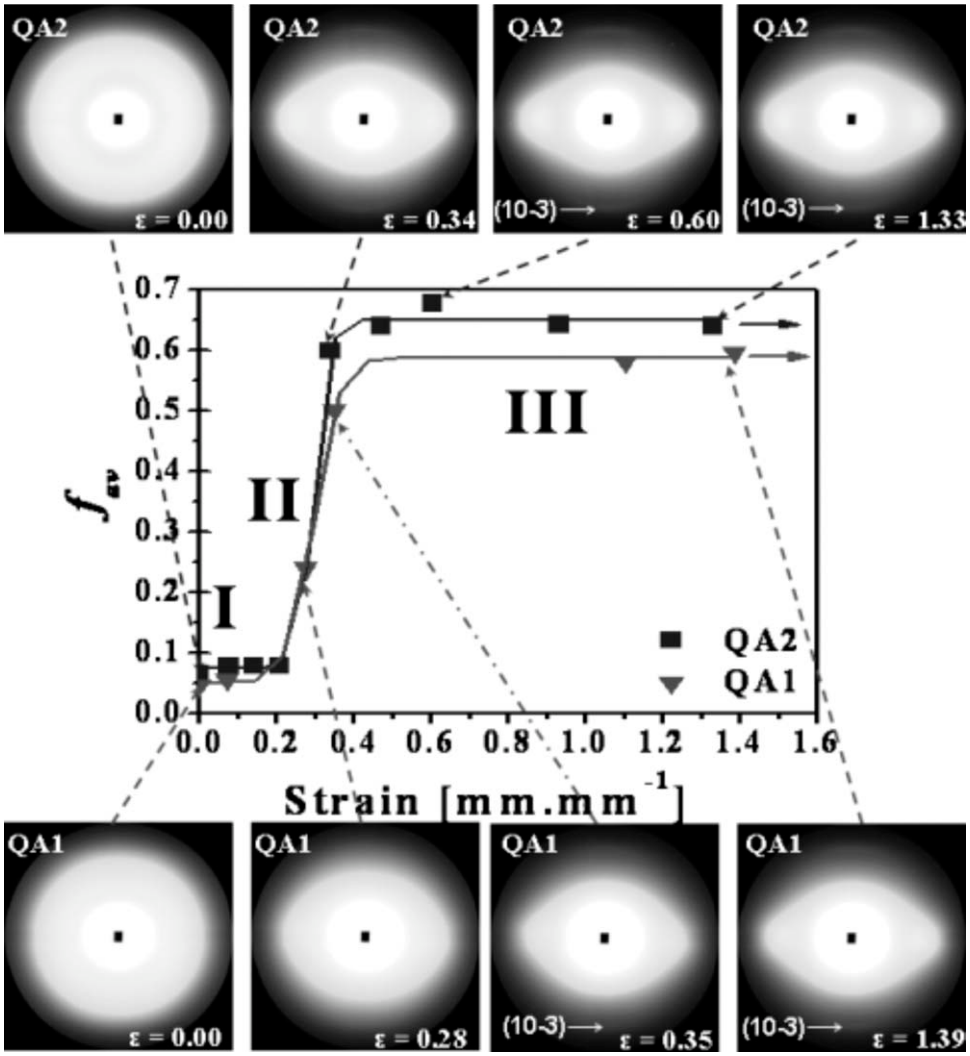

Figure 1 Average polymer orientation, f_{av}, evolution with strain and selected 2D WAXS patterns of samples QA1 and QA2 (fitted by Boltzmann function, $R^2 = 0.99$).

on work of Salem,[2,3] the contribution of the lattice distortion is likely to be small.

RESULTS AND DISCUSSION

Structural evolution from quasi-amorphous morphologies

Figure 1 shows the evolution of the average polymer orientation, $f_{av,}$ as a function of the strain applied, together with the 2D WAXS patterns acquired along the stretching process of QA samples. Both samples are following similar pathways on the f_{av}—strain curve and show similar 2D WAXS patterns. The curve follows a trend of three stages. In the first stage, the average polymer orientation remains almost constant as the strain increases. Suddenly, there is a fast increase of the average polymer orientation, at relatively low change in strain, remarking the stage II. Finally, in stage III, a plateau on the orientation is reached, that is maintained till the end of the deformation process. These stages are identified in the Figure 1 by I, II, and III, respectively. Along the stage I there is no change in 2D WAXD patterns, remaining as a typical amorphous diffraction ring, which becomes elliptic-like shape during the stage II and transforms into two diffused spots on the equator, which intensifies and reduces in area, during the stage III. In this stage, the emerging of the mesomorphic meridional reflection (10−3) peak is observed. The results are suggesting an analogous way of structural evolution of QA morphology, despite the slightly greater orientation attained by QA2 in the stage III, perhaps due to the slightly higher initial orientation of this sample (see Table I).

Equatorial and the meridional intensity versus 2Θ profiles extracted from the 2D WAXS patterns are depicted in Figure 2. Distinct equatorial reflection peaks of amorphous PET, at about $2\theta \approx 19^\circ$, is observed for both QA samples till the end of stage I

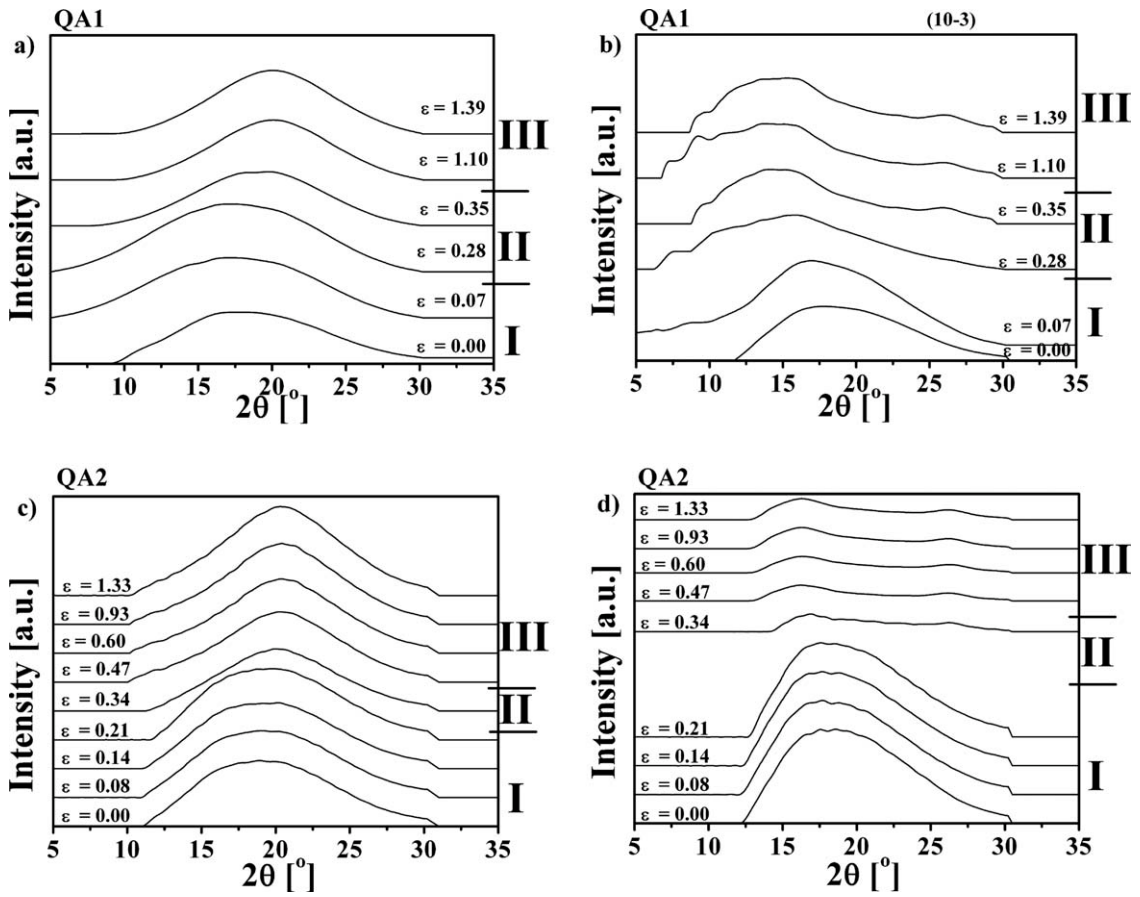

Figure 2 Linear intensity profiles extracted from 2D WAXS patterns: (a) equatorial and (b) meridional of QA1; (c) equatorial and (d) meridional of QA2.

[Fig. 2(a,c) for QA1 and QA2, respectively]. As the stretching is progressing, in stage II, this peak intensifies and concentrates at an angle of $2\theta \approx 20^\circ$. During the stage III only an increase in intensity is observed. The meridional profiles, shown in Figure 2(b,d), undergoes an intensification of the isotropic (amorphous) meridional peak at about $2\Theta \approx 18^\circ$ during stage I. In the stage II this peak shifts to a smaller angle around $2\Theta \approx 16^\circ$, following the appearance of the mesomorphic peak (10−3) at about $2\Theta \approx 26^\circ$. It is important to note that the shift observed in the equatorial profile from $2\theta \approx 19^\circ$ to $2\theta \approx 20^\circ$ is coincident with the appearance of the mesomorphic peak, in the meridional profile. The I-2θ profiles do not show any new feature along stage III.

Phase's mass fractions and amorphous phase orientation evolution as function of strain are plotted in the Figure 3, Figure 3(a) corresponds to QA1 and (b) to QA2, respectively. As can be seen, the amorphous phase orientation evolution curves have identical shape with the average polymer orientation ones (Fig. 1). The main features of phase's evolution are as follow: in stage I, there is a small decrease of amorphous phase due to its transformation into mesophase. In stage II, rapid transformation of great amount of amorphous phase into mesophase is observed and part of the mesophase is organized into periodical mesophase. Such fast phase transformations are taking place simultaneously to the rapid increase of amorphous phase orientation. Finally, in stage III, a higher content of ordered phases is observed, i.e., mesophase and periodical mesophase that reduce steadily in amount during strain, at constant maximum amorphous phase orientation level. This anticipates some destruction/conversion of the ordered phases during deformation (eventually by chain slippage).

The two QA samples are following the same trends, as described previously; nevertheless, since the initial portion of mesophase in QA1 was greater than in QA2 sample, it originated a greater amount of periodical mesophase, during stretching. In solid state, the deformation of QA morphologies did not lead to crystallization, but only to periodical mesophase formation, due to the low mobility of the polymeric chains.

The structural evolution during stretching in solid state of QA precursors can be summarized as follows: (i) stage I, starts when the deformation is initiated and is characterized by a constant level of f_{am},

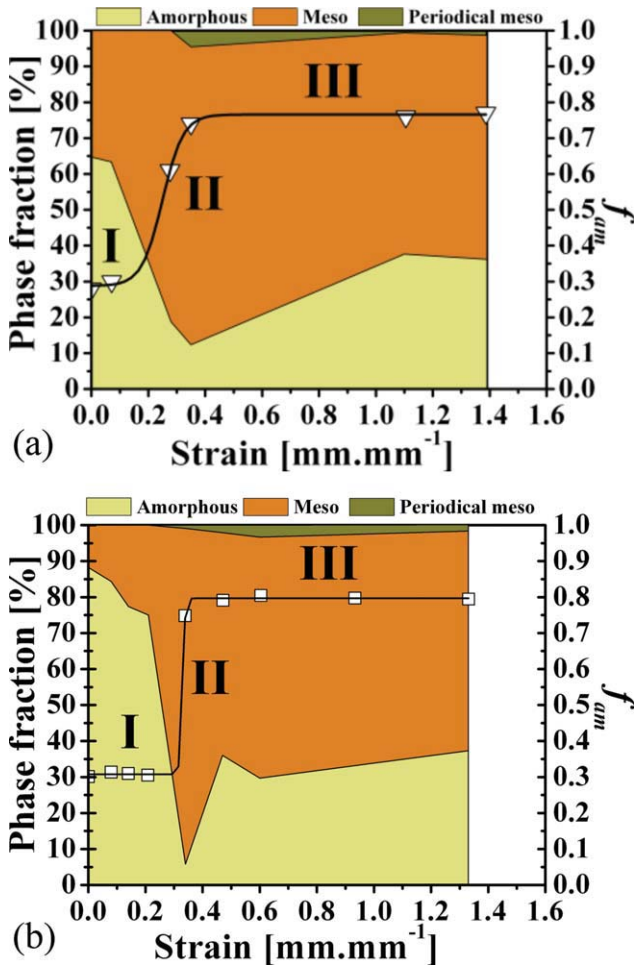

Figure 3 Phase's mass fractions and amorphous phase orientation, f_{am}, evolution of samples: (a) QA1 and (b) QA2 (fitted by Boltzmann function amorphous phase orientation curves, $R^2 = 0.99$). [Color figure can be viewed in the online issue, which is available at wileyonlinelibrary.com.]

and no notable changes in the 2D WAXD patterns, remaining as a typical amorphous hallow. Only a small intensification of the equatorial and the meridional intensity profiles, at constant peak position, is observed together with a negligible amount of amorphous phase fraction transforming into mesophase. At the strain level applied in stage I, it would be expected an earlier transition of the stage I to stage II, due to neck formation. Thus the lack of structural evolution at such strains might be interpreted by the neck formation somewhere along the tensile dumbbell-like bar, out of the region where the 2D WAXS patterns were acquired. Nevertheless, it is expected the neck formation to lead to a slight polymer orientation, however that could be completely recovered when the stretching is stopped, suggesting the absence of a long range network, which could constrain the amorphous chains from relaxing at this strain level in QA morphology. (ii) Further, stretching leads to the beginning of the second stage, stage II, which is characterized by a sharp increase of the amorphous orientation and by the appearance of two spots on the equator in the 2D WAXD patterns. The beginning of this stage is marked by the shift of the meridional peak position to minor angles, followed by the appearance of the meridional peak at about 26°, corresponding to the appearance of the periodical mesophase and by the simultaneous shift of the equatorial peak at $2\theta \approx 19°$ to $2\theta \approx 20°$ (marking already the end of this stage and the beginning of stage III).[10,40,51] The rapid increment of polymer chain orientation leads to a rapid phase transformation from amorphous to mesophase and the appearance of the first signs of organization of the mesophase into periodical one. This fast structural evolution can be attributed to the neck propagation along the center of the tensile bar, where WAXS investigation was carried out. Thus the tensile bar lateral shrinkage induces a considerable polymer chains alignment into the stretching direction, resulting into much oriented/entangled amorphous phase, which is able to transform into mesophase. On the other hand, in consequence of neck propagation, a part of oriented mesophase evolves into periodical one, as result of its orientation and ordering. At this strain level, the polymer chains relaxation is hindered, during the stops of the stretching protocol, due to greater orientation of polymer bulk. The stage III starts when the polymeric chains achieve a plateau on the molecular orientation, which is maintained till the end of the stretching process. This stage is characterized by the presence of an equatorial peak at about $2\Theta \approx 20°$, and two meridional peaks corresponding to the isotropic and mesomorphic phases that are maintained with no position alterations in the intensity scans. Typical of this stage is ordered phases transformation into less ordered one, namely periodical mesophase into mesophase and respectively, mesophase into highly oriented amorphous one. This may be the result of relaxation that is taking place during stretching stops or of the destruction of ordered phases during the progress of deformation (e.g., by chain slippage). In terms of macro deformation, this stage is related to the tensile bar homogeneous deformation through necking propagation.

Structural evolution from semicrystalline morphologies

The average polymer orientation evolution with strain, for both SC specimens, is depicted in Figure 4, with respective 2D WAXD patterns. As observed, there is a considerable difference in the behavior of both samples that is caused by the difference in the initial morphological state of each one (see Table I). For SC1, originally having a 2D crystalline order,

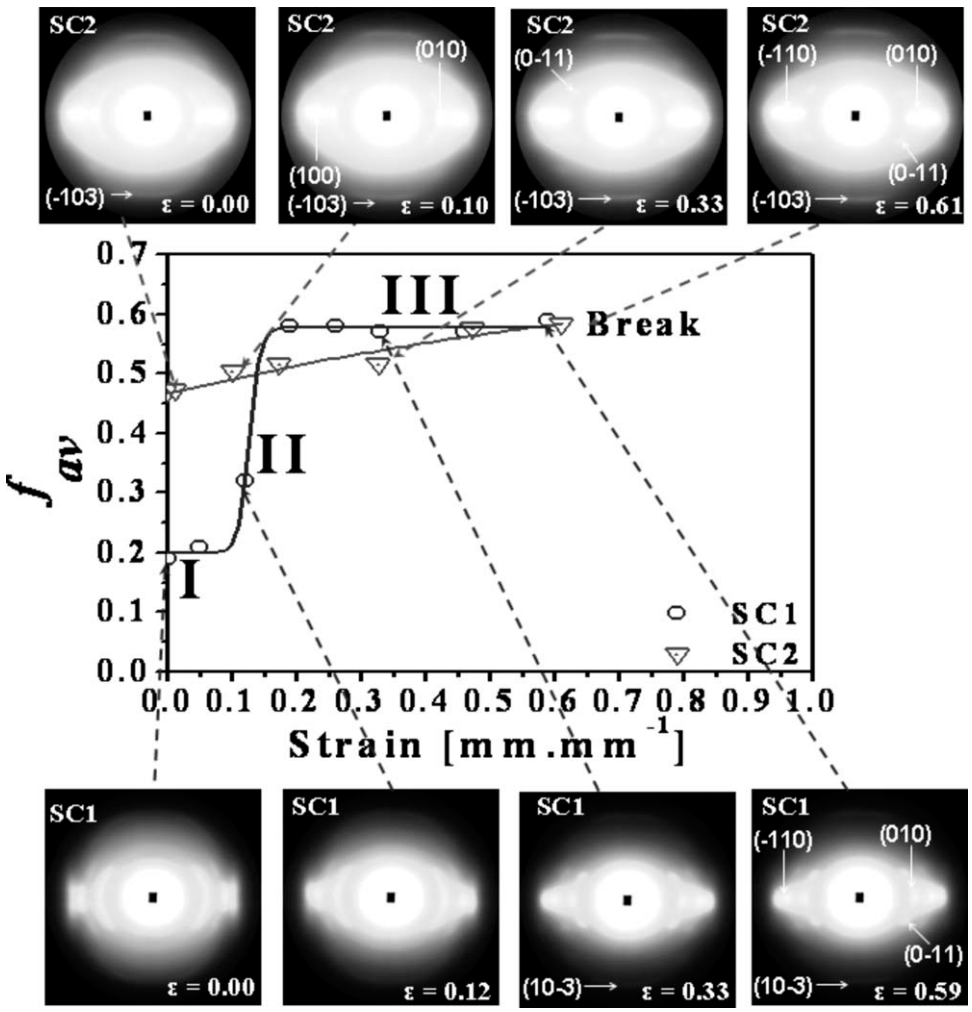

Figure 4 Average polymer orientation, f_{av}, and selected 2D WAXS patterns collected during the stretching of SC1 (fitted by Boltzmann function, $R^2 = 0.99$) and SC2.

the average polymer orientation evolves through three distinct stages, likewise to QA ones. On the other hand, in specimen SC2 with 3D crystalline order, the average polymer orientation increases linearly as the deformation is applied.

SC1 stages can be defined as follow: (i) stage I, occurring at initial part of deformation, features a constant level of orientation, with no notable change in the 2D WAXS patterns, (ii) stage II follows with a sharp increase of orientation level, for small changes of deformation. In addition, there is the intensification of the three main equatorial crystalline reflections, i.e., (010), (−110), (100) of 2D WAXS patterns, and (iii) finally, stage III, begins when the sample reaches the plateau of maximum level of orientation along with the intensification of the principal PET peak reflections, and the emergence of the (−103) meridional peak. This meridional peak is referred as descriptive of the 3D crystalline order.[42,49]

SC2 sample average polymer orientation rises continuously with the strain till breakage of the tensile bar occurs. The 2D WAXS patterns show intensification of PET reflections as well as the appearance and definition of other reflections.

Different initial morphologies of SC1 and SC2 lead to unequal pathway of evolution, but to similar final level of average polymer orientation. Moreover, SC1 develops a 3D crystalline order likewise SC2.

Equatorial and meridional intensity profiles of SC1 and SC2 are shown in Figure 5. In SC1, three distinct PET unit cell reflections are visible, i.e., (010) at $2\theta = 17.3°$, (−110) at $2\theta = 22.5°$, and (100) at $2\theta = 25.7°$. These peaks correspond to the lattice planes parallel to the molecular *c*-axis of PET triclinic unit cell.[14] SC2 shows, (010), (−110), and (100) reflection, however (−110) and (100) reflections appear overlapping as a result of the tendency of the crystallographic plane (100) to align preferentially to the stretching direction.[51] Observing the meridional intensity profiles, it might be noted that SC2 [Fig. 5(d)] exposed a small peak reflection assigned to the (−103) plane of unit cell (at $2\Theta = 26°$) indicative for 3D crystalline order, which is only appearing in stage III of SC1's I-2Θ profiles. In common for both

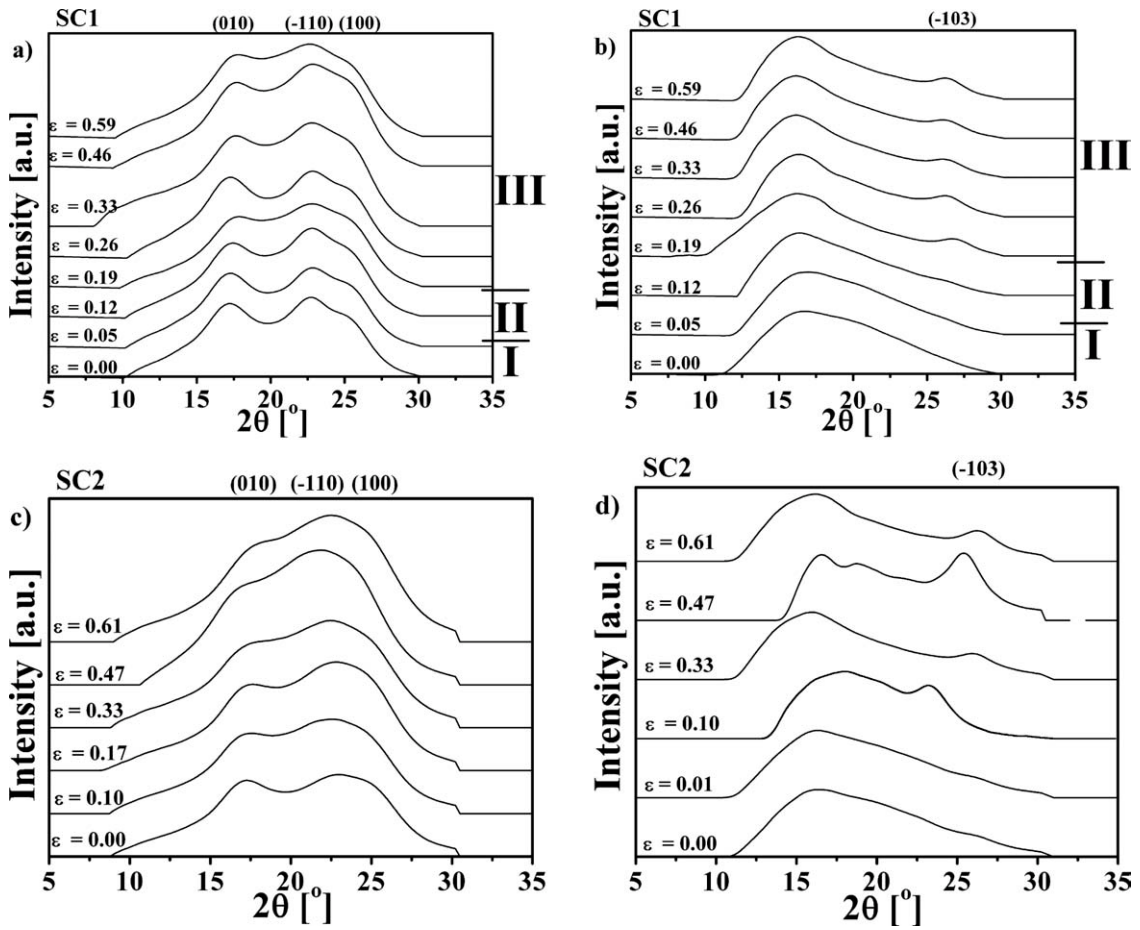

Figure 5 Linear intensity profiles extracted from 2D WAXS patterns: sample SC1 (a) equatorial and (b) meridional, and sample SC2 (c) equatorial and (d) meridional.

SC I-2θ profiles evolution is the intensification of the equatorial and meridional profiles with stretching progress.

Evolution of I-2θ profiles of the SC1 sample is described by stages as follows: the main characteristics of stage I is shift of the meridional peak to the lower angle and its narrowing; further stretching leads to start of stage II, where meridional peak narrows and alters to about $2\Theta = 16°$; along the last stage, stage III, its beginning is marked by appearance in the meridional profiles of (−103) crystalline peak reflection, at about $2\theta = 26.8°$, while the isotropic peak narrows without alteration of its position. Further stretching, along stage III, leads to slight alteration of both meriodional peaks positions, i.e., isotropic to angle of about $2\Theta = 16.3°$ and crystalline one respectively, to around $2\Theta = 26.3°$.

SC2 equatorial profiles evolution [Fig. 5(c)] is distinguished by amplification of the (−110) peak at strain of 0.47 mm mm^{-1}. On the other hand, the meridional profile features a broad isotropic peak around $2\theta = 16°$ and a weak crystalline peak (−103) at about $2\theta = 26.2°$ (see also Fig. 4). This peak moves during the stops of stretching protocol, evidencing the crystallite longitudinal order changes and its sensibility to macromolecular chains extension/relaxation.

Phase's mass fraction, as well as the amorphous and crystalline phases orientation evolution with deformation, for both SC samples is shown in Figure 6. During stage I, SC1 sample features an increase of the amorphous phase mass fraction as a result of some mesophase relaxation concomitant with a decrease upon the crystalline phase orientation is also observed. Thereafter, both amorphous and crystalline phase's orientations increase until the end of stage II, being accompanied by the reduction of the amorphous phase mass fraction and the increase of mesophase. Along stage III, the amorphous and crystalline phase's orientations are maintained constant at its maximum level. A small decrement of the mesophase mass fraction is observed due to its transformation into amorphous phase at alike crystalline phase content, similar to the QA morphologies

In the case of SC2 [Fig. 6(b)], it is observed the continuous increase of mesophase content with strain due to amorphous phase fraction reduction

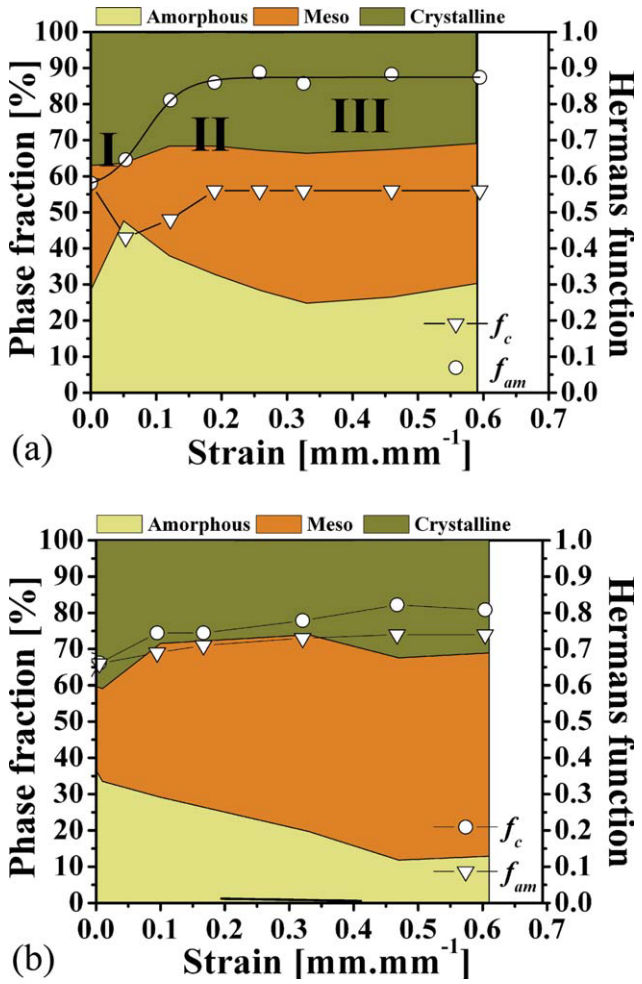

Figure 6 Phase's mass fractions and amorphous, f_{am}, and crystalline, f_c, phases orientations evolution for samples: (a) SC1 (f_{am} results fitted by Boltzmann function, $R^2 = 0.99$) and b) SC2. [Color figure can be viewed in the online issue, which is available at wileyonlinelibrary.com.]

and some crystalline phase relaxation, which is concomitant to the steady increase of amorphous and crystalline phase orientation levels until sample breakage. At ultimate strain levels, just before rupture, minor increase of crystalline phase is observed, as a result of a mesophase reduction; also some mesophase relaxation into amorphous phase is taking place. The 3D crystalline order of SC2 hinders chains relaxation, leading to a linear increase of the polymer bulk orientation (both amorphous and crystalline phases) levels with strain progress. In contrast, for sample SC1, such behavior is only observed during stage III, when the crystalline phase reaches the 3D order.

The apparent crystal sizes, normal to the three crystal reflections planes, (100), (010), and (−103), were estimated by the analysis of the linear intensity profiles taken across the reflection peaks, using the Scherrer equation [eq. (6)]. These results are shown in Figure 7(a,b) for SC1 and SC2 samples, respectively. The three chosen reflections planes are almost orthogonal to each other, thus marking the average lateral sizes of the crystallites induced by deformation.

The SC1 samples crystallites sustain the following directional changes along the stages [Fig.7(a)]: stage I—the crystallites show two dimensional order with no change on its dimensions. Crystallites become slightly larger along the stage II. This may be attributed to some rotation of the benzene rings within the crystallites. The start of stage III is marked by appearance of (−103) peak corresponding to longitudinal order (3D crystalline order), which causes shrinkage of frontal plane (100) at stable lateral size, (010) due to rearrangement of the benzene stacking. Along the stage III, the crystallites undergo reorganization by a slight frontal enlargement, followed by longitudinal contraction, till sample breakage.

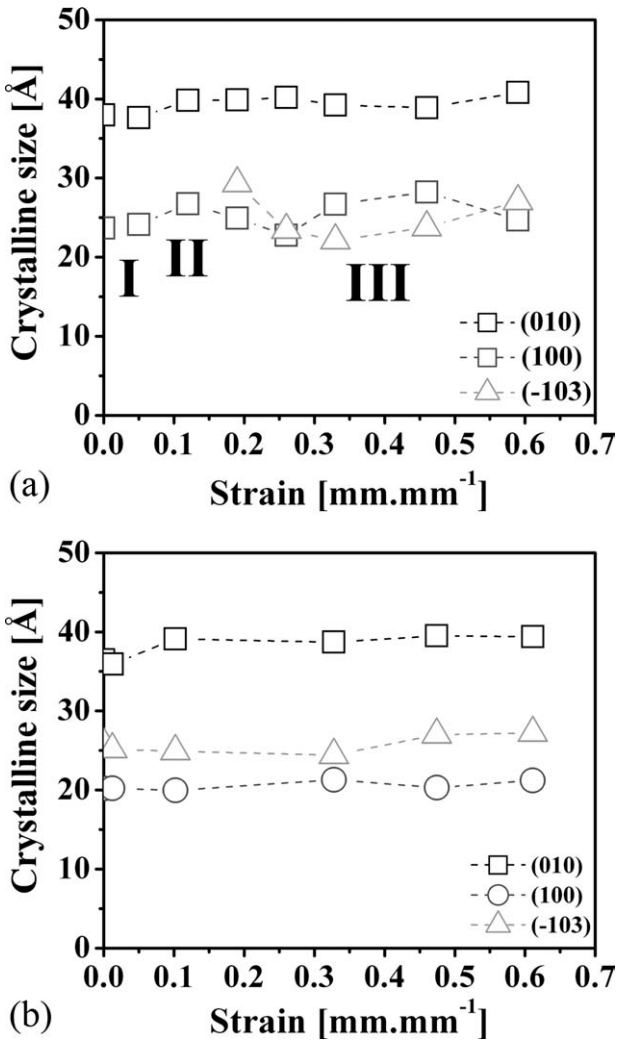

Figure 7 Changes of estimated crystal size from three nearly orthogonal planes, (010), (100), and (−103) calculate by Scherer equation during uniaxial deformation of: (a) SC1 and (b) SC2.

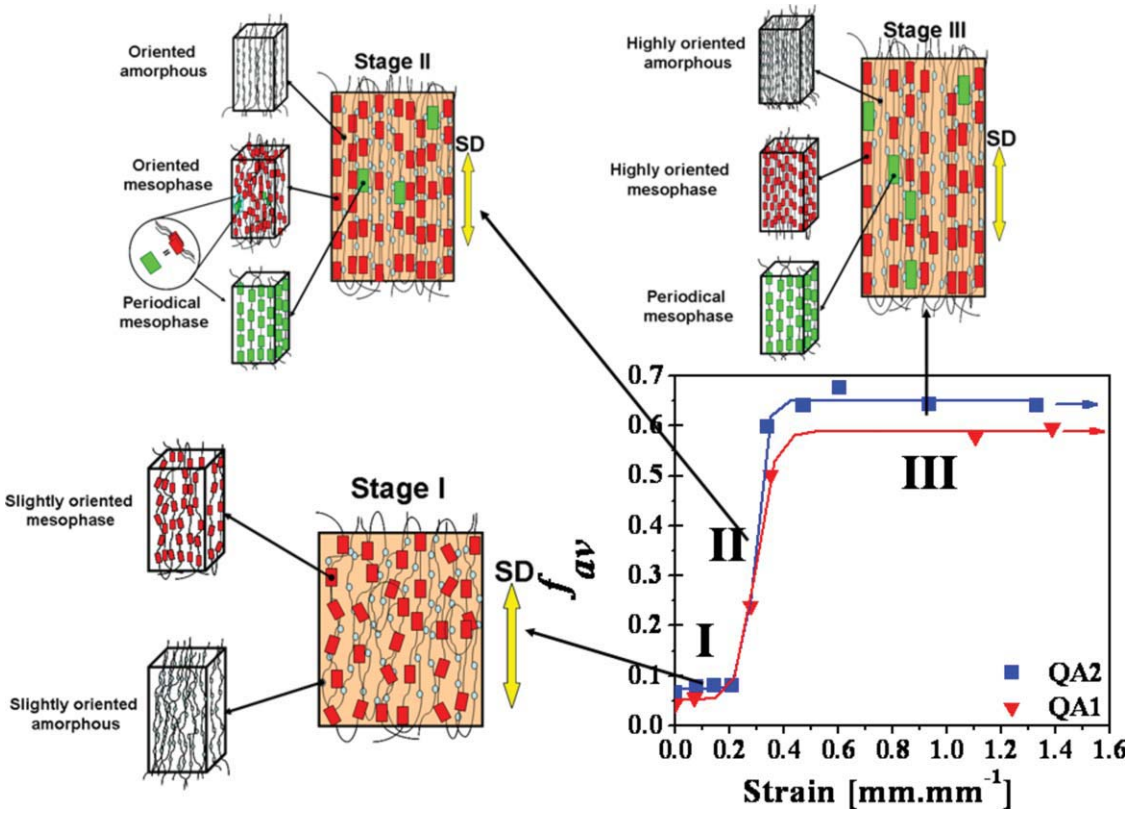

Figure 8 Schematic diagrams to illustrate the structure evolution during solid-state stop uniaxial stretching of PET with QA morphology. [Color figure can be viewed in the online issue, which is available at wileyonlinelibrary.com.]

The SC2 has a crystalline phase with three dimensional order, from the start, defined by the crystalline reflection (−103). In this case, there is a slight laterally enlargement of (010) during the first steps of stretching protocol, followed by stable crystallite sizes till sample breakage [Fig. 7(b)].

Crystallites with 2D order prior to deformation (samples SC1) result in significant variation of its size along stretching protocol, whereas with 3D crystalline order (SC2 morphology) shows only slight change of its size.

The solid-state structural evolution of SC morphologies that have not reached the 3D crystalline order (SC1) can be summarized as follows:

Stage I corresponds to a stable average polymer orientation level, while the amorphous phase orientation rapidly increases and orients. This behavior occurs during the first stop of deformation of the step deformation applied and is associated to the mesophase relaxation. The crystalline orientation level declines along the stage I, but the crystalline phase content does not change, as well as the crystallite sizes. This might be related to a taut polymer bulk, causing a decrement of the crystallite orientation. In terms of macroscopic deformation, during stage I, neck forms somewhere along the tensile bar, out of incident point of X-ray beam, contributing to the relatively poor structural evolution. During stage II, neck propagates and the X-ray beam coincides on that region. The average of amorphous and crystalline phase orientation rises rapidly, causing a decrease of amorphous phase due to its transformation into mesophase. Crystallites with 2D order enlarge slightly in the frontal (010) and lateral (100) sides. Stage III is characterized by a plateau of maximum orientation level, i.e., average, amorphous, and crystalline phases orientation, at alike crystalline phase content. The mesophase fraction improves as a result of amorphous phase consumption. Such structure evolution is suggestive for deformation of tensile bar through necking. At the beginning of stage III, (−103) peak reflection appears, showing the formation of longitudinal order associated with frontal enlargement of the crystallites. At the last part of the stage III, crystallites feature longitudinal shrinkage till sample rupture.

The morphology of SC2 specimen with strain progress evolves by constant increase of the level of orientation (i.e., average polymer, amorphous, and crystalline) promoting the evolution of intermediate mesophase as result of decline of amorphous phase at almost invariable crystalline phase content. Such behavior might be attributed to immediate neck propagation and following homogeneous lengthening through necking.

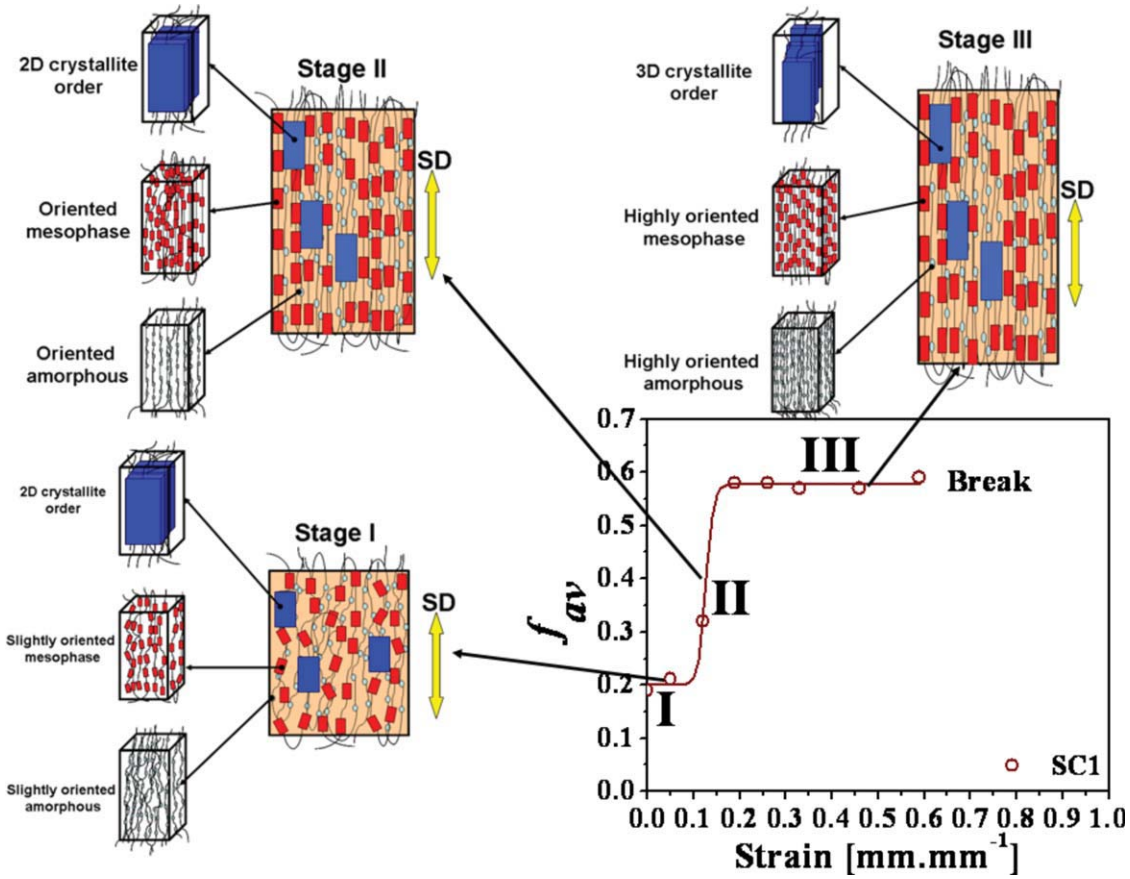

Figure 9 Schematic diagrams to illustrate the structure evolution during solid-state stop uniaxial stretching of PET with SC morphology with 2D crystalline order. [Color figure can be viewed in the online issue, which is available at wileyonlinelibrary.com.]

Structural models

Based on the experimental observations mentioned above, some structural models depicting the structural hierarchy or structural evolution mechanism from different initial morphologies, in the solid state, are proposed. In Figure 8, it is represented the structural evolution mechanism for QA morphologies, whereas in Figures 9 and 10, the models for the SC precursors with 2D and 3D crystalline order are shown, respectively.

Structural evolution from quasi-amorphous precursors

Figure 8 represents the structural evolution of QA samples. At the initiation of deformation, QA samples consist of slight oriented amorphous phase and mesophase, and their proportion changes into more mesophase throughout stage I at constant orientation level. Stage I ends and stage II begins when the polymer chain orientation rapidly increases and a large amount of amorphous phase is transformed into mesophase. Since the orientation has increased, a small fraction of mesophase is developed into periodical mesophase, as a result of the overlapping of the mesophase chains perpendicular to the stretching direction. As deformation further proceeds, the polymer chains approach their extensibility limit, leading to leveling-off of the average polymer orientation. This is called stage III. Here, a part of the periodical mesophase relaxes into mesophase and further into amorphous one, maintaining the same level of orientation. This can be explained by the untying of mesophase polymer chains surrounded by tight polymer bulk, which transforms them into highly oriented amorphous phase. These samples are not able to crystallize during deformation.

Structural evolution from semicrystalline precursors with 2D crystalline order

The mechanism responsible for the strain-induced structural changes in the solid state of the SC sample with 2D crystalline order can be summarized using the structural model illustrated in Figure 9. Stage I is described by initially constant average polymer molecular orientation level, out of the necking region. As the stretching progresses, initially slightly oriented polymer bulk evolves by increasing

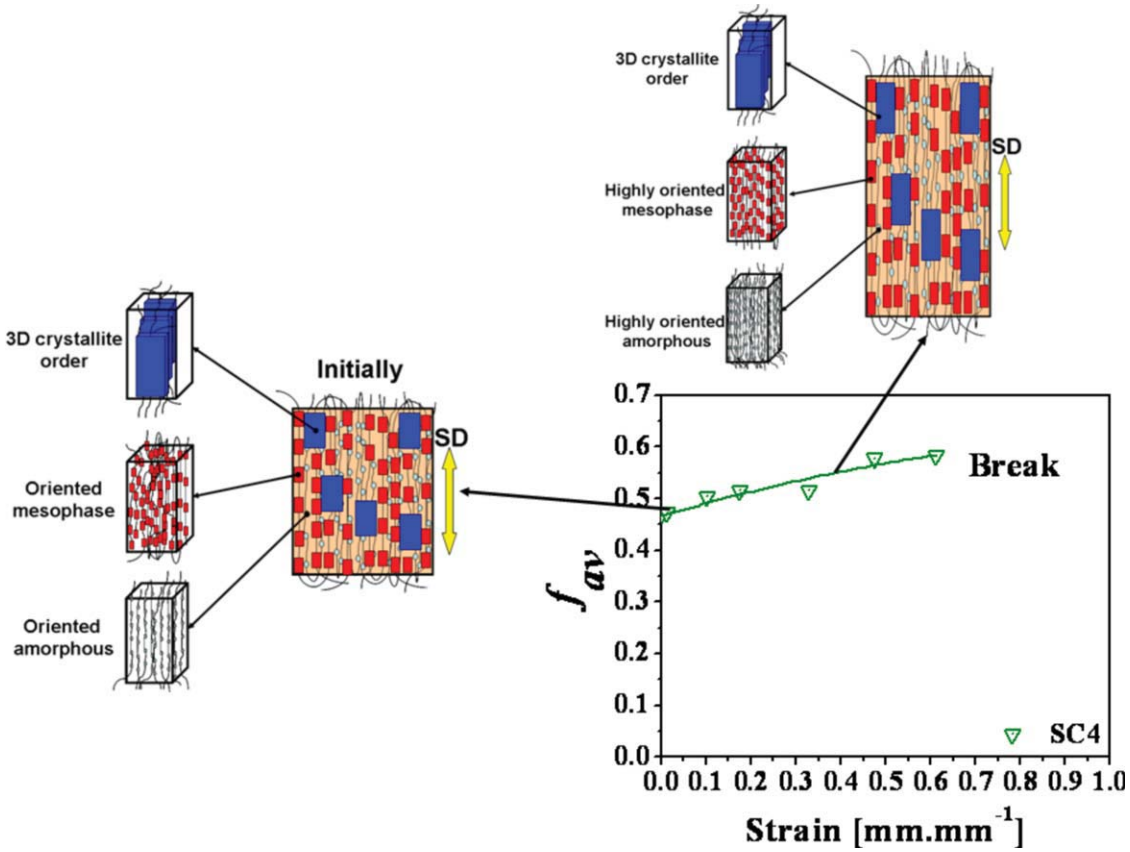

Figure 10 Schematic diagrams to illustrate the structure evolution during solid state stop uniaxial stretching of PET with SC morphology with 3D crystalline order. [Color figure can be viewed in the online issue, which is available at wileyonlinelibrary.com.]

amorphous phase portion due to some mesophase relaxation. A small amount of crystalline phase also relaxes into mesophase. A raise in the average polymer orientation, leading to mesophase increase is observed in stage II, at necking. Along this stage crystallites feature enlargement of frontal and lateral side's parameters, owing to tightening of polymer amorphous matrix. Further stretching causes the polymer chains orientation approaching its extensibility limits that results in a plateau of maximum polymer orientation, recognized as stage III. This orientation level contributes for the development of 3D ordered crystalline phase and increment of mesophase, mainly because of amorphous phase transformation. Along this stage, the crystallites with 3D order grow into the stretching direction.

Structural evolution from semicrystalline precursors with 3D crystalline order

For SC2 samples with 3D crystalline order, the structure evolution and average polymer orientation with strain progress is illustrated in Figure 10**.** The strain-induced phase transitions involved mainly mesophase formation from oriented amorphous phase and some from crystalline phase relaxation. Average polymer orientation increases with the increase of strain, until maximum chain extensibility is reached. During the first steps of the stretching protocol crystallites laterally enlarge, where after feature a stable crystallite size till sample rupture.

CONCLUSIONS

The evolution of strain-induced phase transition and average polymer molecular orientation with strain increment was investigated for different initial morphological states of PET. QA and SC morphologies show distinct structure evolutions during stretching. Distinct structural models were proposed for each type of initial morphology, interpreting the obtained experimental results.

Solid-state structural evolution upon deformation is strongly dependent on the initial state of the material. Initially amorphous samples evolve into highly oriented ones that are not able to crystallize, although a high level of average polymer molecular orientation is achieved. They are formed of highly oriented chains in different phases (amorphous, mesophase, and periodical mesophase) whose mass fractions evolve during stretching, as a result of

subsequent chain stretching/slippage and relaxation phenomena. A SC precursor gives rise to a final structure where a 3D crystalline order is attained, even when starting with 2D crystalline order. In all cases, the final average molecular orientation level attaint is independent of the initial morphological state. Its evolution follows three stages, for any kind of samples that has not achieved a 3D crystalline order: firstly there is a small plateau of constant molecular orientation (stage I) until neck formation, followed by quick rise (stage II), that than stabilizes in a new plateau of maximum molecular orientation during necking propagation through the specimen (stage III). For 2D crystalline precursor, crystallite size enlarges during initial deformation stages, and then evolves due to rearrangements of benzene ring stacking during stretching. A 3D crystalline precursor (SC2) leads to a continuous evolution of the average molecular orientation with strain until break, without almost no crystalline phase evolution.

Initially, morphological distinct PET samples show different structural evolutions during stretching and also markedly distinct mechanical behaviors.

References

1. Fakirov, S. Handbook of Thermoplastic Polymers: Homopolymers, Copolymers, Blends, and Composites; Wiley-VCH Verlag GmbH: Weinheim, 2002.
2. Salem, D. R. Polymer 1992, 33, 3189.
3. Salem, D. R. Polymer 1992, 33, 3182.
4. Bonart, R. Kolloid-zeitschrift and zeitschrift fur polymere 1966, 213, 1.
5. Bonart, R. Kolloid Zeitschrift and Zeitschrift fuer Polymere 1969, 231, 438.
6. Salem, D. R. Polymer 1994, 35, 771.
7. Goschel, U. Polymer 1996, 37, 4049.
8. Salem, D. R. Polymer 1995, 36, 3605.
9. Chevalier, L. M. Y. Mech Mater 2007, 596.
10. Ajji, A.; Cole, K. C.; Dumoulin, M. M.; Brisson, J. Polymer 1995, 36, 4023.
11. Ajji, A.; Guevremont, J.; Cole, K. C.; Dumoulin, M. M. Polymer 1996, 37, 3707.
12. Ajji, A.; Cole, K. C.; Dumoulin, M. M.; Ward, I. M. Polym Eng Sci 1997, 37, 1801.
13. Goschel, U. Polymer 1995, 36, 1157.
14. Goschel, U.; Deutschert, K.; Abetzt, V. Polymer 1996, 37, 1.
15. Goschel, U.; Urban, G. Polymer 1995, 36, 3633.
16. Adams, A. M.; Buckley, C. P.; Jones, D. P. Polymer 2000, 41, 771.
17. Smith, M. R.; Cooper, S. J.; Winter, D. J.; Everall, N. Polymer 2006, 47, 5691.
18. Gowd, E. B.; Ramesh, C.; Byrne, M. S.; Murthy, N. S.; Radhakrishnan, J. Polymer 2004, 45, 6707.
19. Morawiec, J.; Bartczak, Z.; Pluta, M.; Galeski, A. J Appl Polym Sci 2002, 86, 1426.
20. Vigny, M.; Tassin, J. F.; Gibaud, A.; Lorentz, G. Polym Eng Sci 1997, 11, 1785.
21. Gorlier, E.; Haudin, J. M.; Billon, N. Polymer 2001, 42, 9541.
22. Dargent, E.; Grenet, J.; Dahoun, A. Polym Eng Sci 1997, 37, 1853.
23. Martins, C. I.; Cakmak, M. Polymer 2007, 48, 2109.
24. Mahendrasingam, A.; Martin, C.; Fuller, W.; Blundell, D. J.; Oldman, R. J.; Harvie, J. L.; MacKerron, D. H.; Riekel, C.; Engstrom, P. Polymer 1999, 40, 5553.
25. Blundell, D. J.; Mahendrasingam, A.; Martin, C.; Fuller, W.; MacKerron, D. H.; Harvie, J. L.; Oldman, R. J.; Riekel, C. Polymer 2000, 41, 7793.
26. Mahendrasingam, A.; Blundell, D. J.; Martin, C.; Fuller, W.; MacKerron, D. H.; Harvie, J. L.; Oldman, R. J.; Riekel, C. Polymer 2000, 41, 7803.
27. Blundell, D. J.; MacKerron, D. H.; Fuller, W.; Mahendrasingam, A.; Martin, C.; Oldman, R. J.; Rule, R. J.; Riekel, C. Polymer 1996, 37, 3303.
28. Chaari, F.; Chaouche, M.; Doucet, J. Polymer 2003, 44, 473.
29. Chaari, F.; Chaouche, M. J Polym Sci Part B Polym Phys 2004, 42, 1915.
30. Kolb, R.; Seifert, S.; Stribeck, N.; Zachmann, H. G. Polymer 2000, 41, 2931.
31. Kawakami, D.; Ran, S.; Burger, C.; Fu, B.; Sics, I.; Chu, B.; Hsiao, S. B. Macromolecules 2003, 36, 9275.
32. Matthews, R. G.; Ajji, A.; Dumoulin, M. M.; Prud'homme, R. E. Polymer 2000, 41, 7139.
33. Mahendrasingam, A.; Martin, C.; Fuller, W.; Blundell, D. J.; Oldman, R. J.; MacKerron, D. H.; Harvie, J. L.; Riekel, C. Polymer 2000, 41, 1217.
34. Mahendrasingam, A.; Blundell, D. J.; Wright, A. K.; Urban, V.; Narayanan, T.; Fuller, W. Polymer 2003, 44, 5915.
35. Kawakami, D.; Ran, S.; Burger, C.; Avila-Orta, C.; Sics, I.; Chu, B.; Benjamin, S. H.; Kikutani, T. Macromolecules 2006, 39, 2909.
36. Kawakami, D.; Burger, C.; Ran, S.; Avila-Orta, C.; Sics, I.; Chu, B.; Chiao, S.-M.; Hsiao, B. S.; Kikutani, T. Macromolecules 2008, 41, 2859.
37. Daubley, R.; Bunn, C. W.; C.J, B. Proc R Soc London Ser A 1954, 226, 531.
38. Auriemma, F.; Corradini, P.; De Rosa, C.; Guerra, G.; Petraccone, V.; Bianchi, R.; Di Dino, G. Macromolecules 1992, 25, 2490.
39. Asano, T.; Balta Calleja, F. J.; Flores, A.; Tanigaki, M.; Mina, M. F.; Sawatari, C.; Itagaki, H.; Takahashi, H.; Hatta, I. Polymer 1999, 40, 6475.
40. Parravicini, L.; Leone, B.; Auriemma, F.; Guerra, G.; Petraccone, V.; Dino, G. D.; Bianchi, R.; Vosa, R. J Appl Polym Sci 1994, 52, 875.
41. Ran, S.; Wang, Z.; Burger, C.; Chu, B.; Hsiao, B. S. Macromolecules 2002, 35, 10102.
42. Kawakami, D.; Ran, S.; Burger, C.; Fu, B.; Sics, I.; Chu, B.; Hsiao, S. B. Macromolecules 2003, 36, 9275.
43. Todorov, L. V.; Martins, C. I.; Viana, J. C. J Appl Polym Sci 2011, 120, 1253.
44. Teixeira, D. S.; Fonseca, J.; Pontes, A. J.; Sepúlveda, A. T.; Cortez, J.; Viana, J. C. Micro Mechanics; Europe University of Minho: Guimarães, Portugal, 2007; p 345.
45. Todorov, L. V.; Viana, J. C. Int J Mater Forming 2008, 1, 661.
46. Oultache, A. K.; Kong, X.; Pellerin, C.; Brisson, J.; Pezolet, M.; Prud'homme, R. E. Polymer 2001, 42, 9051.
47. Stribeck, N. X-Ray Scattering of Soft Matter; Springer: Berlin, Heidelberg, New York, 2007.
48. Wilchinsky, Z. W. J Appl Phys 1960, 31, 1969.
49. Kawakami, D.; Hsiao, B. S.; Ran, S.; Burger, C.; Fu, B.; Sics, I.; Chu, B.; Kikutani, T. Polymer 2004, 45, 905.
50. Kawakami, D.; Hsiao, B. S.; Burger, C.; Ran, S.; Avila-Orta, C.; Sics, I.; Kikutani, T.; Jacob, K. I.; Chu, B. Macromolecules 2005, 38, 91.
51. Alvarez, C.; Sics, I.; Nogales, A.; Denchev, Z.; Funari, S. S.; Ezquerra, T. A. Polymer 2004, 45, 3953.